Antarctic Science 30(6), 379–393 (2018) © Antarctic Science Ltd 2018 doi:10.1017/S0954102018000391

Estimating surface melt and runoff on the Antarctic Peninsula using ERA-Interim reanalysis data

JULIANA COSTI[1,6], JORGE ARIGONY-NETO[2], MATTHIAS BRAUN[3], BULAT MAVLYUDOV[4], NICHOLAS E. BARRAND[5], ALINE BARBOSA DA SILVA[2], WILIAM CORREA MARQUES[6] and JEFFERSON CARDIA SIMÕES[1]

[1]*Centro Polar e Climático, Instituto de Geociências, Universidade Federal do Rio Grande do Sul, Porto Alegre, Brazil*
[2]*Laboratório de Monitoramento da Criosfera, Instituto de Oceanografia, Universidade Federal do Rio Grande, Rio Grande, Brazil*
[3]*Institut für Geographie, Friedrich-Alexander-University Erlangen-Nürnberg, Wetterkreuz 15, D-91058 Erlangen, Germany*
[4]*Russian Academy of Sciences, Institute of Geography, Vavilova, 37, Moscow, Russia*
[5]*School of Geography, Earth and Environmental Sciences, University of Birmingham, Birmingham, UK*
[6]*Laboratório de Análise Numérica e Sistemas Dinâmicos, Instituto de Matemática, Estatística e Física, Universidade Federal do Rio Grande, Rio Grande, Brazil*
juliana.costi@ufrgs.br

Abstract: Using the positive degree days approach and ERA-Interim reanalysis downscaled data, the researchers ran a melt model spatially gridded at 200 m with annual temporal resolution over 32 years and estimated surface melt (SM) and surface runoff (SR) on the Antarctic Peninsula. The model was calibrated and validated independently by field measurements. The maximum surface melt values occurred in 1985 (129 Gt), and the maximum runoff (40 Gt) occurred in 1993; both parameters showed minimum values in 2014 (26 Gt and 0.37 Gt, respectively). No significant trends are present. Two widespread positive anomalies occurred in 1993 and 2006. The results reveal that the floating ice areas produce an average of 68% of runoff and 61% of surface melt, emphasizing their importance to coastal hydrography. During the seven years preceding the Larsen B collapse, surface melt retention was higher than 95% on floating ice areas, and negative runoff anomalies persisted. Excluding the islands, the vicinity of this former ice shelf exhibits the highest specific surface melt and runoff across the studied area.

Received 16 September 2017, accepted 14 September 2018

Key words: positive degree days, glacier and snow surface melting, meltwater

Introduction

The Antarctic Peninsula (AP) is a region that is warming far faster than the global average. During the second half of the 20th century the annual mean air temperature increased by 2.5–3.0 °C (Vaughan *et al.* 2003, Turner *et al.* 2005, Trenberth *et al.* 2007, Steig *et al.* 2009). The number of days with positive air temperature and consequently the duration of melt events every year have increased at a rate of 0.5 ± 0.3 days yr^{-1} over the 1980–2002 period (Torinesi *et al.* 2003). This climatic scenario increases surface melt, which accelerated over the 20th century (Abram *et al.* 2013). Since the millennium, a significant cooling trend was observed (Turner *et al.* 2016) that also has glaciological implications (Oliva *et al.* 2017).

Surface melt has been regarded as one of the major factors associated with the breakup and disintegration of the Larsen A and B ice shelves (Scambos *et al.* 2003). Surface runoff (SR) from land-based ice masses directly and indirectly influences short-term sea level changes. It adds freshwater to the oceans and lubricates the glacier bed, causing potential changes in, and acceleration of, the glacier mass flux (Pfeffer *et al.* 1991, Zwally *et al.* 2002, Vaughan 2006, Osmanoglu *et al.* 2014). Recent studies have shown that ocean temperature is the leading factor that determines large ice shelves' thinning (Pritchard *et al.* 2012). The resulting decreased buttress (Fürst *et al.* 2016), in turn, accelerates the ice flux of marine-terminating glaciers, resulting in a dynamic thinning much larger than the losses caused by surface melt (Wouters *et al.* 2015). Though not the main contributors to mass loss and ice shelf breakup, surface melt and runoff are strongly associated with the observed changes on the AP.

Surface melt, surface runoff and ice discharge from glaciers by calving are the main drivers for freshwater input in the surrounding oceans of the AP. Freshwater supplies are important components in coastal ecosystems because they influence the physical and chemical settings of the water column, affecting both the structure and the function of coastal food webs (Moline *et al.* 2004). Studies in shallow, circulation-restricted bays of King George Island showed that suspended particulate matter transported by glacier runoff can reduce light availability in shallow waters (Schloss *et al.* 2012) and governs the availability of macronutrients for

phytoplankton production (Nędzarek 2008, Kienteca Lange *et al.* 2014). Even far from the coast, Dierssen *et al.* (2002) found phytoplanktonic blooms to be associated with glacier melt. Hodson *et al.* (2017) reported the occurrence of biologic activity hotspots associated with iron enrichment supplied by glacial weathering.

Previous studies investigated surface melt and runoff on AP primarily through remote sensing and regional climate modelling. Using passive microwave data (1978–present), studies addressing changes in melt extent, duration and water quantities could not find a significant temporal trend. However, these studies note decreasing, though statistically insignificant, trends for melt extent, melt index and total annual melt (Torinesi *et al.* 2003, Liu *et al.* 2006, Kuipers Munneke *et al.* 2012, Trusel *et al.* 2013). The only positive trend in melt duration was found by Torinesi *et al.* (2003) from 1980–2000. They found that melting lasts for an average of 50 days on the AP, reaching a maximum of 100, with an increasing trend of 0.5 ± 0.3 day yr^{-1} (1980–1999). Liu *et al.* (2006) determined a median melt duration of 59 days with an absolute variation of 5.39 days and a melt extent ranging from 2.5×10^5–3.5×10^5 km^2. Barrand *et al.* (2013) combined remote sensing observations and simulations from the regional model RACMO2 to investigate melt conditions, finding melt extents ranging from 2.8×10^5–3.3×10^5 km^2 (QuickSCAT) and 1.8×10^5–3×10^5 km^2 (RACMO2 regional atmospheric model) from 2000–2009.

Quantitative estimates of melt rates or freshwater input to the ocean are even scarcer. Van de Berg *et al.* (2005) showed a maximum annual melt of 0.5 m water equivalent (w.e.) yr^{-1} occurring on the Larsen Ice Shelf's northern edge from 1958–2002. Vaughan (2006) estimated values for surface melt in the year 2000 of 54 ± 26 Gt (450 ± 216 mm w.e.). He considered only the grounded ice portion of the AP and predicted an increase in surface melt to 100 ± 46 Gt by 2050, assuming the current increasing trend of annual mean air temperature. Hock *et al.* (2009) estimated that from 1961–2004, an increase in the sea level of 0.22 ± 0.16 mm yr^{-1} resulted from the contribution of mass loss from glaciers and ice caps surrounding Antarctica, mostly AP. More recently, Kuipers Munneke *et al.* (2012) found surface melt values ranging from 20–130 Gt yr^{-1} for the AP. The analysis considered the entire Antarctic ice sheet and surrounding ice shelves, from 1979–2009, and showed no statistically significant decreasing trend.

This study presents comprehensive estimates for surface melt and runoff on the Antarctic Peninsula and surrounding islands. It uses a positive degree day-based glacier melt model adapted from Vaughan (2006) and Pfeffer *et al.* (1991), driven by data from the global reanalysis project ERA-Interim (ERAI) from the European Centre for Medium-range Weather Forecast (ECMWF). The model is calibrated and validated via a multi-criteria scheme using *in situ* observations and long-term surface mass balance (SMB) records. The model covers the period 1981–2014.

Study site

The AP is a region with strong latitudinal and longitudinal gradients of climatic parameters (Morris & Vaughan 2003). The central mountain range, reaching more than 2000 m a.s.l., forms a major obstacle in the southern hemisphere polar vortex (Fig. 1). The climate of the AP west coast and adjacent islands is cold maritime, while the conditions are much more continental on the east coast and further south. Consequently, summer melt regularly occurs along the west coast at lower elevations. Frequent warm foehn-type winds on the east coast are known to cause considerable surface melt, and cold barrier winds lead to cold air mass outbreaks from the Filchner-Ronne Ice Shelf along the AP's mountains to the north. Such foehn events impact the surface temperature regionally in timescales varying from hours to seasons (Cape *et al.* 2015). Larsen C&D, Wilkins and George VI ice shelves are the largest low-elevation areas. The plateau of the Antarctic Peninsula is dominated by a dry snow zone, with mean annual surface temperatures below -11°C (Rau & Braun 2002). Large mountain glaciers drain from the plateau to both sides of the AP. The small islands surrounding the peninsula are covered by ice caps and ice fields.

Data

The AP does not have a well-distributed weather station network with long time series (see Fig. 1). Under these circumstances, a feasible alternative to the spatial interpolation of uneven observations is to use data provided by reanalysis projects. Such datasets incorporate available observations to minimize the errors of the prediction model.

ERAI is a reanalysis product from ECMWF. It provides data from 1979–present with a finest spatial resolution of approximately $0.25^o \times 0.25^o$. Compared with previous versions, such as ERA-40 and ERA-15, the temperature bias over Antarctica has been reduced. The orography in the model is an average of finer resolution digital elevation models, such as GTOPO30 (Gesch *et al.* 1999). This averaging smooths the highly complex topography of the AP.

To better represent the topography, the RAMP DEM (Liu *et al.* 2015) was used as the input for an altitudinal lapse-rate downscaling method, which was evaluated using near-surface air temperature data from 28 weather

https://doi.org/10.1017/S0954102018000391 Published online by Cambridge University Press

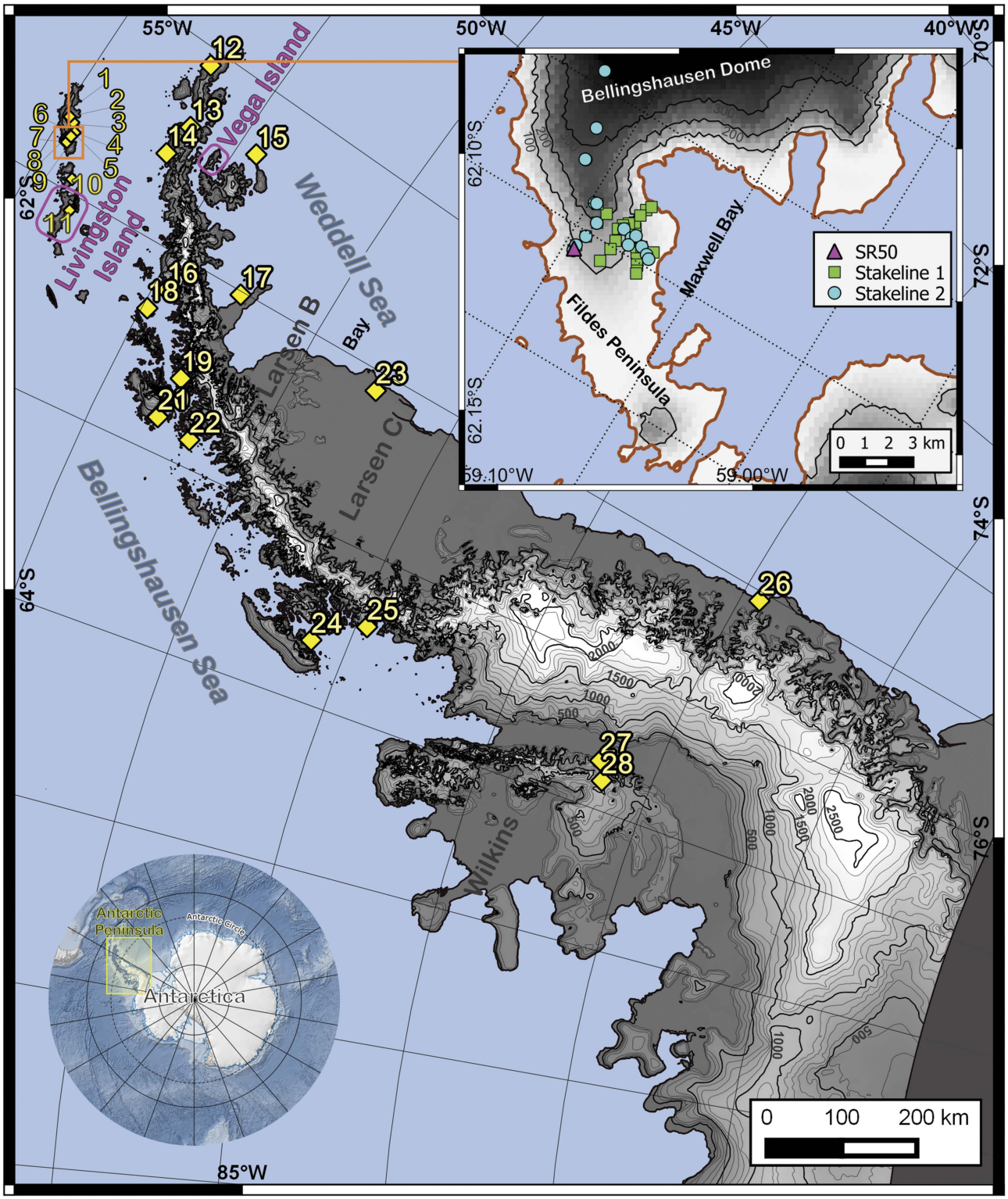

Fig. 1. Map showing the study area and data-source distribution. Elevation contours are extracted from RAMP-DEM (Liu *et al.* 2015). Weather stations are represented by yellow diamonds and labelled with numbers, as shown in Table II. The top right detailed map of King George Island shows the glaciological stakes and ultrasonic ranger used for calibration and validation in the Bellingshausen Dome and the Fildes Peninsula. Magenta squares show locations in Livingston and Vega islands, where long-term surface mass balance records are available.

https://doi.org/10.1017/S0954102018000391 Published online by Cambridge University Press

stations. The resulting grid cell size after downscaling was 200 m x 200 m.

Direct ablation measurements were available from three sources: 1) Measurements in 10–14 day intervals at 29 mass balance stakes during the summer from 2007–2012 at the Bellingshausen Dome in King George Island, South Shetland Islands (stake line 1) (Table I; Mavlyulov 2014), 2) continuous surface melt measurements available from a sonic ranging sensor (SR50) operated over 42 days of the 1997/98 summer at daily intervals (Braun *et al.* 2001, Braun & Hock 2004), 3) mass balance stakes readings during summer field campaigns (stake line 2). These measurements were conducted during two summer seasons (1997/1998 and 1999/2000) on the Bellingshausen Dome (Braun *et al.* 2001, Braun & Hock 2004).

Spatially-integrated summer and winter mass balances of the Hurd and Johnsons glaciers in Hurd Peninsula, Livingston Island were available for ten years (Navarro *et al.* 2013, data provided by the World Glacier Monitoring System). A 14-year record of the annual surface mass balance of Glaciar Bahía del Diablo, Vega Island was used as a quantitative reference for the north-eastern AP region (Skvarca *et al.* 2004, Marinsek & Ermolin 2015).

Methods

ERA-Interim temperature downscaling

To account for the spatiotemporal variation in the air temperature altitudinal lapse rates along the study area, the temperature and geopotential height differences between the 1000 hPa and 750 hPa pressure levels were computed. Thereafter, the ratio between the two differences for each day and grid element was calculated, and the given lapse rate (Eq. (1)) was applied to the elevation difference between the RAMP-DEM and the ERAI geopotential height at the surface (Eq. (2)). The result was then reduced from the temperature at 2 m (Eq. (3)).

$$lr(\varphi,\lambda,d)=\frac{T_{1000}(\varphi,\lambda,d)-T_{750}(\varphi,\lambda,d)}{h_{1000}(\varphi,\lambda,d)-h_{750}(\varphi,\lambda,d)} \quad (1)$$

$$dh=h_{ERA-sfc}-h_{RAMP-DEM} \quad (2)$$

and

$$T_{DS}(\varphi,\lambda,d)=T_{2m}(\varphi,\lambda,d)+(dh(\varphi,\lambda,d)*lr(\varphi,\lambda,d)), \quad (3)$$

where lr is the lapse rate, T_{1000}, T_{750}, h_{1000} and h_{750} are the temperatures and geopotential heights at 1000 hPa and 750 hPa, respectively, $h_{ERA\text{-}sfc}$ is the geopotential height of the surface, $h_{RAMP\text{-}DEM}$ is the elevation given by RAMP DEM (Liu *et al.* 2015), T_{DS} is the temperature downscaled, T_{2m} is the temperature 2 m above the surface, φ and λ are the latitude and longitude, and d is the day. For each model grid cell, the ERAI cell with the cell centre closest to the model grid centre was used.

It is worth noting that the lapse-rate method for air temperature downscaling only accounts for the decrease of the air temperature due to the vertical variation inside the ERA-Interim grid elements. It does not include any further dynamic processes that may affect the air temperature which are not already represented in the ERA-interim global climatic model. It also represents the free atmosphere and does not account for any local effects or boundary-layer processes.

Surface melt and runoff computations

The positive degree day (PDD) is the sum of daily positive near-surface air temperatures during a given period (in this case, one year) (Vaughan 2006). When multiplied by a melt factor (m), it provides the total surface melt (M):

$$M(\phi,\lambda,\tau)=m\sum_{d=1}^{d=365}T_{DS}(\phi,\lambda,d)\alpha(\phi,\lambda,d) \quad (4)$$

$$\begin{cases}\alpha(\phi,\lambda,d)=1, if\ T_{DS}(\phi,\lambda,d)>0\\ \alpha(\phi,\lambda,d)=0, if\ T_{DS}(\phi,\lambda,d)\le 0\end{cases}$$

Table I. Data used for the calibration and validation of the surface melt and runoff model.

Dataset	Type	Period of measurement	Location	Elevation range (m a.s.l.)	Usage	Reference
Weather station (see Table II)	Meteorological Records (see Table II)	Variable (see Table II)	Variable	Variable	Cal	NOAA
Stake line 1	29 ablation stakes	2007–2012	KGI	54–261	Cal	Mavlyulov (2014)
Stake line 2	22 ablation stakes	1997/1998 1999/2000	KGI	85–300 85–205	Val	Braun *et al.* (2001, 2004)
SR50	Ultrasonic ranger	02/12/1997–02/01/1998	KGI	85	Val	Braun *et al.* (2001, 2004)
SMBs	Summer, integrated	2001–2011	LIV	0–370	Val	Navarro *et al.* (2013)
SMBw	Winter, integrated	2001–2011	LIV	0–370	Val	Navarro *et al.* (2013)
SMBa	Annual, integrated	1999–2014	VI	75–630	Val	Skvarca *et al.* (2004) Marinsek & Ermolin (2015)

KGI denotes King George Island, LIV: Livingston Island, VI: Vega Island, Cal: calibration data, Val: validation data.

https://doi.org/10.1017/S0954102018000391 Published online by Cambridge University Press

where $d = 1$ is the first day of the annual melting periods (assumed to 1 October in this case) and τ is the year.

The energy balance at the surface implies that melt can occur when the air temperature is equal to or below 0 °C, and even not occur when the temperature is positive. In this sense, the 0 °C threshold for melt occurrence may be considered an artificial threshold. In order to determine the more suitable threshold, the model was used to consider five different thresholds for the same period covered by the work of Barrand *et al.* (2013), i.e. from 1999–2002. The mean melt duration of the period as estimated by our model was then compared against the QuickSCAT-derived estimates obtained by Barrand *et al.* (2013). The classical PDD approach considers that melt occurs when the air temperature is positive. The work presented here also explores melt when the air temperature is equal to and above 0 °C, above -1°C, above -0.5 °C, above 0.5 °C and above 1 °C. The latter two thresholds were tested in order to account for the known overestimation of the ERAI-derived air temperature on the AP.

Surface runoff (Q) is calculated as the difference between surface melt and the amount of meltwater retained in the snowpack through refreezing, pore filling and capillarity (M_0):

$$Q = M - M_0 \tag{5}$$

with M_0 given by (Pfeffer *et al.* 1991) as

$$M_0 = \frac{c}{L} C T_f + (C - M)\left(\frac{\rho_{pc} - \rho_c}{\rho_c}\right), \tag{6}$$

where c is the heat capacity of ice, L is the latent heat of fusion of ice, C is the snow accumulation, T_f is the temperature of the firn at the beginning of the melt season (in positive Celsius degrees below the freezing point), ρ_c is the initial firn density (taken as 400 kg m^{-3}) and ρ_{pc} is the pore close-off density (taken as 830 kg m^{-3}). After setting $\rho_c = 400$ kg m^{-3} and $\rho_{pc} = 830$ kg m^{-3} (Vaughan 2006), one gets:

$$M_0 = \left(0.003 T_f + 0.52\right) C. \tag{7}$$

After assuming that T_f is the mean air temperature of the previous year in each grid cell, the only unknown variable for calculating M_0 is C. C is approximated as the annual accumulation for each grid element given by ERAI (resampled by nearest neighbour to the model grid). Hence, the accumulation and temperature-driven changes in retention for each year is estimated, and the surface runoff is estimated using Eq. (5).

Calibration and validation of the model

A multi-criteria calibration and validation scheme was applied, with rigorous data splitting for model calibration, data downscaling and model validation.

To validate the downscaling approach, monthly PDDs that were computed from the downscaled ERAI data and from weather station data (records longer than ten years) were compared. The analysis was restricted to the months from October to March to focus on the melt periods. The PDDs' correlation strength and the sum of errors were utilized as quality indicators.

The melt model was calibrated by tuning the melt factor using ERAI downscaled data in Eq. (4) to achieve an optimal fit to the ablation records (N = 300) of stake line 1. A melt factor of 5.4 mm w.e. K d^{-1} was determined with $r^2 = 0.65$ using all available records. When stakes are considered individually, the melt factor takes values between 2.2 and 12.6 mm w.e. K d^{-1} (although both of these are extreme values). The melt factor is well within the range reported for comparable Arctic regions and at the upper bound for Antarctica (Huybrechts & Oerlemans 1990, Braithwaite & Zhang 2000, Hock 2003).

Independent validation of the model performance was carried out using a variety of datasets at different locations and different time intervals. The melt rates at stake line 2 and the SR50 continuous record were compared over a six-week melt period, both on King George Island. The surface mass balance records provided an integrated error estimate for summer and winter (Livingston Island) (Navarro *et al.* 2013) or an entire glacier mass balance year (Vega Island) (Skvarca *et al.* 2004, Marinsek & Ermolin 2015).

Results

PDD threshold and spatial representation of the mean melt duration (MMD)

By spatially comparing the annual mean melt duration from 1999–2002 (Fig. 2), it can be observed that the best performance is achieved when using the 0 °C threshold. The energy balance at the surface determines that melting can occur at temperatures below 0 °C. However, the comparisons made between the ERAI-derived and the weather stations-derived PDDs (see below and Table II) show that both are very well correlated, although the absolute values are overestimated. This may explain the best performance of the 0 °C threshold for determining the mean melt duration, although it could be expected that a lower temperature would result in a better representation of the mean melt duration.

Downscaling and melt model performance

The ERAID-derived PDDs showed very good agreement with weather station data. Correlation coefficients ranged from 0.58–1.0, with the majority above 0.9 (Table II).

https://doi.org/10.1017/S0954102018000391 Published online by Cambridge University Press

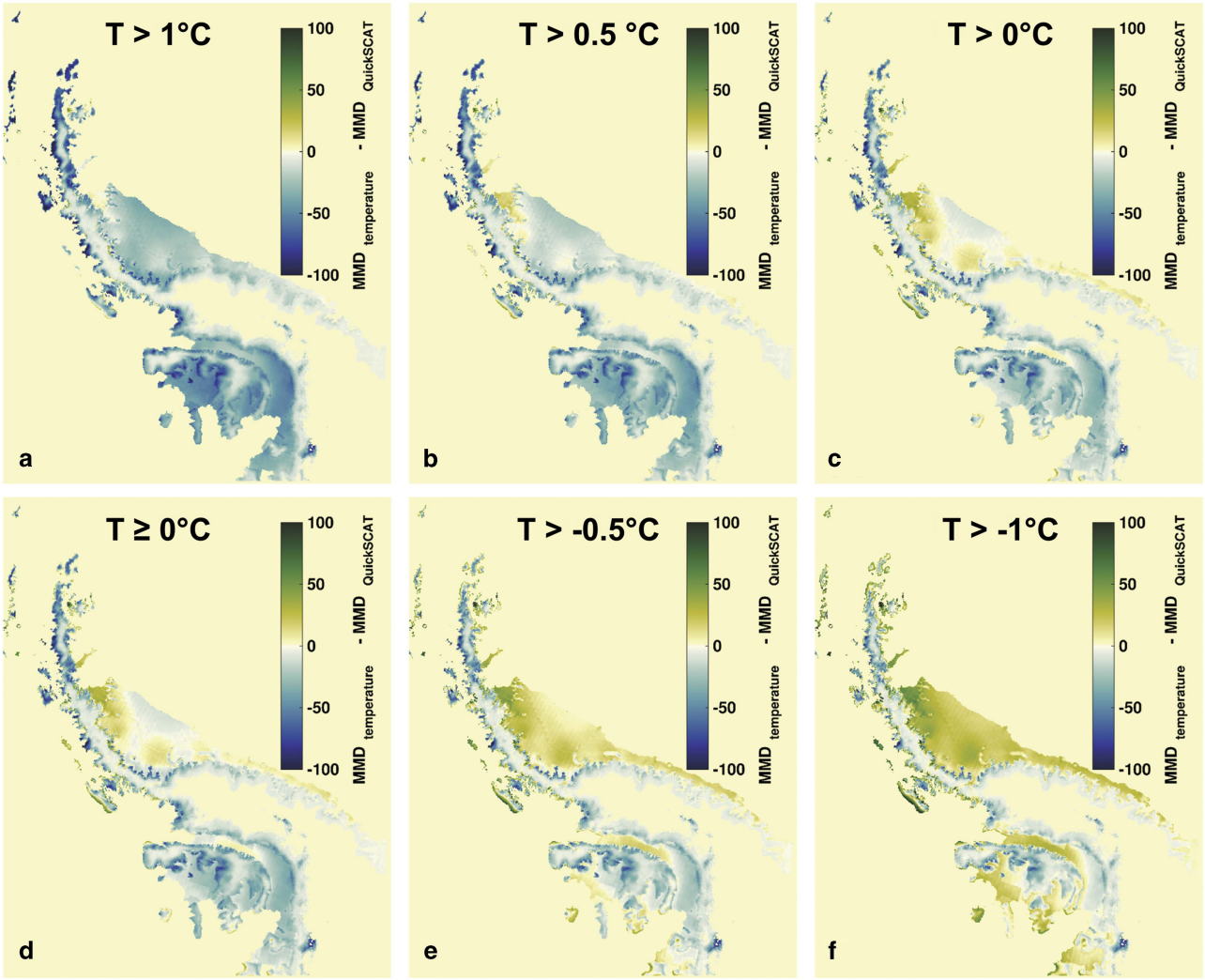

Fig. 2. Comparison of the mean melt duration (MMD) derived from ERAI-based air temperature data against QuickSCAT-derived maps. Six different thresholds are applied to ERAI-derived data to determine the occurrence of melt: **a.** T > 1°C, **b.** T > 0.5°C, **c.** T > 0°C, **d.** T ≥ 0°C, **e.** T > -0.5°C, and **f.** T > -1°C.

Nevertheless, absolute values were overestimated by ERAID-derived data.

The surface melt was validated using two other independent point ablation measurements carried out in the Bellingshausen Dome (stake line 2 and SR50). Compared to these datasets, the modelled surface melt produced a slight underestimation of the surface ablation. After 41 days of ablation monitoring with the SR50, a final difference of 80 mm w.e. was found between the modelled and the measured ablation. The root mean square error (RMSE) was 7.19 mm w.e., and the bias was 4.9 mm w.e. The linear correlation of the ablation estimates with stake line 2 was 0.86 (Fig. 3), with RMSE of 19.08 mm w.e. and bias of 7.14 mm w.e.

The surface melt estimations in the Hurd Peninsula (Livingston Island) were compared to measurements carried out by Navarro *et al.* (2013) on the Hurd Glacier (HG) and Johnsons Glacier (JG) from 2002–2011 (Fig. 4). The same study also measured the winter accumulation, which was used to evaluate the accumulation estimate over the same periods. The correlation of the modelled ablation was 0.61 with HG and 0.68 with JG, with RMSE of 158 mm w.e. The accumulation correlations were 0.8 (HG) and 0.49 (JG), with RMSE of 247 mm w.e. Values always ranged on the same scale and did not show a fixed over- or underestimation. Additionally, the annual surface mass balance of Glaciar Bahía del Diablo (Vega Island) was estimated and compared to field measured data from this site (see Fig. 4). The error was lower than 200 mm w.e. for nine of the 13 analysed years, the correlation between the measured and the modelled SMB was 0.67, and the RMSE was 214 mm w.e.

https://doi.org/10.1017/S0954102018000391 Published online by Cambridge University Press

Table II. Weather stations used in this study for the validation of PDDs estimated from ERAI. The correlation coefficient and RMSE were calculated between monthly PDDs derived from weather station (WS) measurements and ERAI estimation, excluding the months from April to September.

WS label on map	WS name	Latitude	Longitude	Elevation	Period	Number of months	r^2	RMSE
1	Ferraz	62.08°S	58.38°W	18	2008–2011	18	0.96	146.19
2	King George	62.08°S	58.40°W	267	2001–2002	6	1.00	21.48
3	Arctowski	62.16°S	58.46°W	3	1979–1990	67	0.97	147.08
4	Jubany	62.23°S	58.65°W	20	1980–2014	178	0.98	129.79
5	King Sejong	62.21°S	58.75°W	11	1991–2013	137	0.96	130.42
6	Dinamet (Uruguay)	62.17°S	58.83°W	10	1985–2014	171	0.98	95.62
7	Bellingshausen	62.20°S	58.93°W	16	1979–2014	209	0.98	90.30
8	Frei (Base)	62.25°S	58.93°W	10	1979–1985	39	0.99	88.43
8	Frei (Station)	62.25°S	58.93°W	10	1985–2014	174	0.99	67.95
9	Great Wall	62.21°S	58.96°W	10	1985–2014	173	0.98	87.81
10	Arturo Prat	62.50°S	-9.68°W	5	1979–2014	186	0.99	80.11
11	Juan Carlos	62.66°S	60.38°W	10	1989–2014	48	0.90	246.56
12	Joinville Island	63.18°S	55.40°W	75	2007–2013	30	0.97	22.65
13	Esperanza	63.40°S	56.98°W	8	1979–2014	209	0.92	195.08
14	O'Higgins	63.31°S	57.90°W	10	1979–2014	213	0.94	60.52
15	Marambio	64.23°S	56.71°W	198	1979–2014	213	0.93	90.32
16	Primavera	64.17°S	60.95°W	50	1979–1982	19	0.64	110.21
17	Matienzo	64.97°S	60.05°W	32	1979–1987	33	0.96	35.12
18	Racer Rock	64.16°S	61.53°W	17	1991–2006	73	0.92	18.79
19	Gonzalez	64.80°S	62.85°W	10	1981–1982	4	0.98	6.07
20	Palmer	64.76°S	64.08°W	8	1979–2004	97	0.90	225.83
21	Bonaparte Point	64.78°S	63.06°W	8	1997–2014	44	0.97	12.55
22	Faraday/Vernadsky	65.25°S	64.26°W	9	1979–2014	139	0.90	40.52
23	Larsen Ice Shelf	66.96°S	60.55°W	17	1995–2014	115	0.99	6.43
24	Rothera	67.56°S	68.13°W	15	1979–2013	167	0.96	26.96
25	San Martin	68.13°S	67.13°W	4	1979–2014	213	0.84	6.29
26	Butler Island	72.21°S	60.33°W	91	1990–2014	140	0.90	3.16
27	Fossil Bluff	71.33°S	68.35°W	55	1986–2013	74	0.58	0.89
28	Uranus	71.43°S	68.93°W	780	1990–2005	73	0.98	13.44

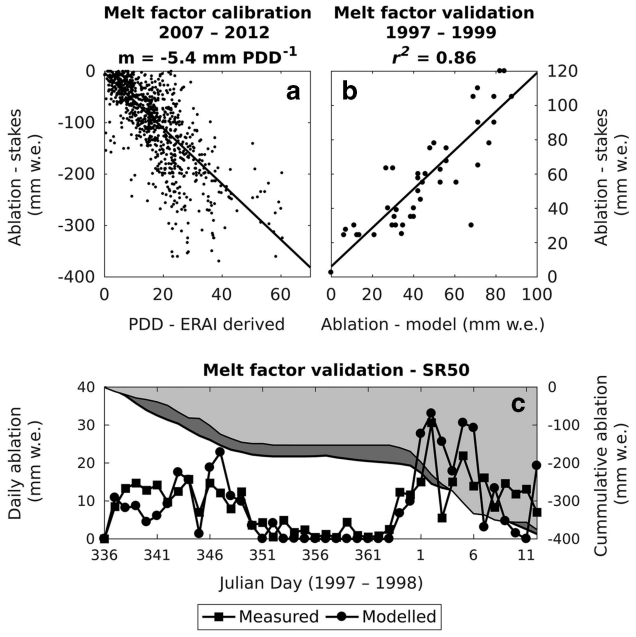

Fig. 3. a. MF estimation, **b.** validation against ablation measured at stake line 2 (1997/1998, 1999/2000) and **c**. SR50 (40 consecutive days, from December 1997 to January 1998).

The average ablation was underestimated in the SR50 and stake line 2 (SL2) validation site, by respectively 0.14 mm w.e. (2% below the observation) and 11.4 mm w.e. (20% above the observation). The average summer ablation of Livingston Island was overestimated by 120.45 mm w.e. (17% above the observation), whereas the winter accumulation was overestimated by 107.69 mm w.e. (16% above the observation). The annual mass balance of the Bahía del Diablo glacier was overestimated by 30.52 mm w.e. (20% above the observation). The best correlation between the modelled and the observed time series was found with the SL2 observations, which is expected because the SL2 is located at the melt factor calibration site. Although the SR50 measurements were also performed at the calibration site, the PDD method is known for its poorer performance on the daily timescale when compared to longer timescales.

The observational data available for validating this study consists of measurements performed in time intervals ranging from daily to annual, implying different magnitudes of ablation, accumulation and mass balance. To account for the diverse measurement magnitudes, the normalized RMSE was computed while considering the range of the observed measurements. The

https://doi.org/10.1017/S0954102018000391 Published online by Cambridge University Press

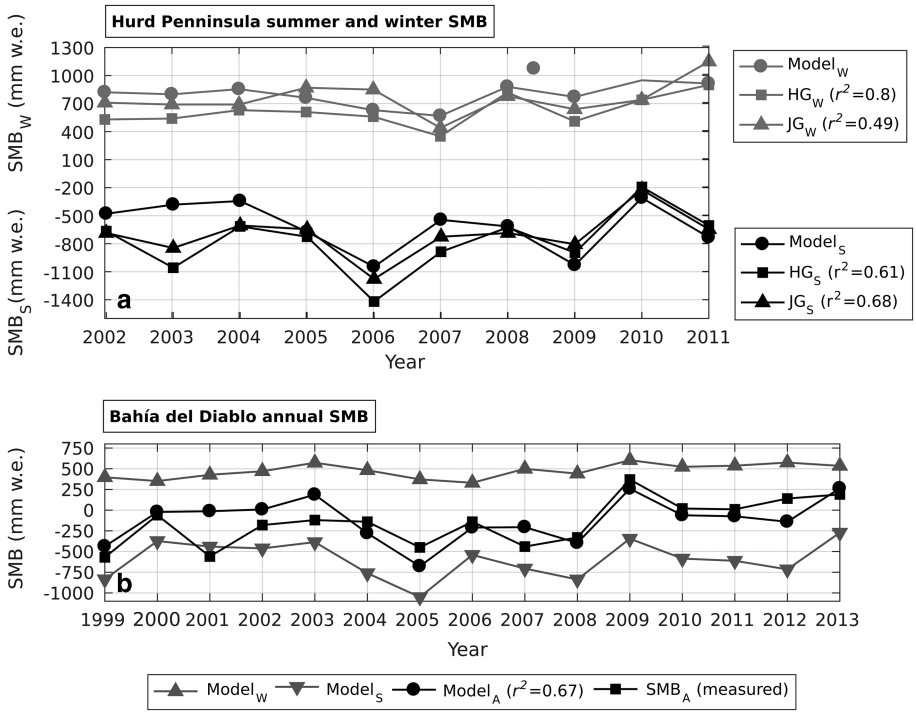

Fig. 4. Comparison of modelled area-averaged SMB in: **a**. the Hurd Peninsula (Livingston Island) with summer and winter SMB from the Hurd (HG) and Johnsons (JG) Glaciers (Navarro *et al.*, 2013) and **b**. Bahía del Diablo Glacier's (Vega Island) annual SMB (Skvarca *et al.*, 2004; Marinsek and Ermolin, 2015).

normalized RMSE ranged from 0.16–0.25, with the lowest value associated with the SL2 validation site and the highest value associated with the winter accumulation on Livingston Island. It was expected that the model would have a worse performance away from the melt factor calibration site because melt factors typically show a large variation in regions as large as the Antarctic Peninsula. However, a better comparison of errors would require longer measurements carried out at similar timescales.

Surface melt and runoff time series

The annual time series for the mean near-surface air temperature and PDDs and the total surface melt (M), M_0 and surface runoff (Q) are presented in Fig. 5 for the total, grounded and floating areas of the AP. The years correspond to the melt season that started in October of the previous year.

The mean near-surface air temperature does not represent the PDDs' interannual variability. Both series show $r^2 = 0.11$, which is not surprising considering that there are no PDDs during most months that compose the annual mean temperature.

Total surface melt had maximum values in 1985 (129 Gt) and 1993 (127 Gt) and a minimum value in 2014 (26 Gt). The mean and standard deviation values for the entire period and area were 75 ± 54 Gt, or 46 ± 15 Gt and 25 ± 8 Gt when separately considering floating and grounded areas, respectively. Surface runoff had a maximum value in 1993 (40 Gt) and a minimum value in 2014 (0.37 Gt), with a mean of 9 ± 8 Gt and, for floating and grounded areas, 5 ± 6 Gt and 3 ± 2 Gt, respectively.

Since 2008, both surface melt and runoff have persistently shown negative anomalies when considering the entire period. The same happened from 1996–2002 but only for surface runoff. The period 1996–2002 is also characterized by a lower interannual variability in the mean air temperature, PDDs and surface melt, whereas M_0 has not shown the same behaviour. Hence, the decoupling of surface runoff and surface melt for this period might be associated with high accumulation rates.

The spatial distribution of the mean and standard deviation of surface melt and runoff is presented in Fig. 6. The effects of foehn winds are clearly reflected in the mean surface melt (Fig. 6a) for the western border of the Larsen C Ice Shelf, showing that these types of events are large and persistent enough to be represented in a global reanalysis.

Surface melt and runoff regions

The study divided the AP in 11 sub-regions (Fig. 7) to analyse the spatial surface melt and runoff variations in the major drainage basins and ice shelves, bays and topographical features. Because the areas (A) of the

https://doi.org/10.1017/S0954102018000391 Published online by Cambridge University Press

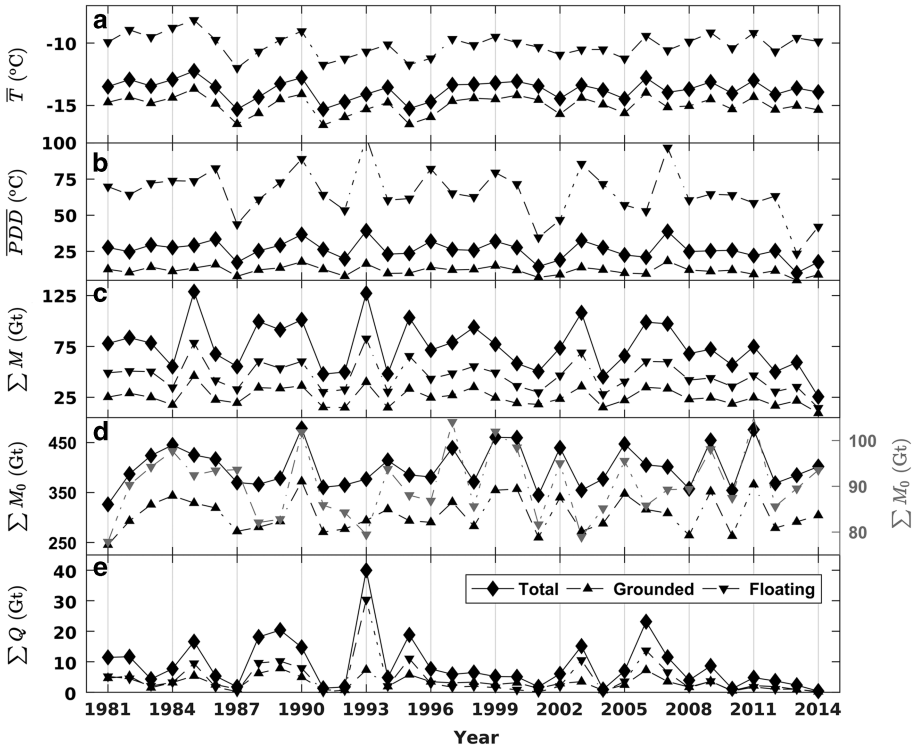

Fig. 5. a. Mean temperature, **b.** mean PDDs, **c.** total surface melt (M), **d.** total potential retention (M_0) and the total surface runoff (Q) annual time series for the total (continuous line, diamonds), grounded ice (dotted line, upward-pointing triangles) and floating ice (dotted line, downward-pointing triangles) areas. In d, the right axis shows scale for the floating area.

regions considered are different, the specific surface melt and runoff (M/A and Q/A, in m w.e.) were computed. The largest specific surface melt and runoff correspond to the South Shetland Islands (SSI). Excluding the islands, specific surface melt and runoff are larger in the E-LB region.

The regional time series have a higher correlation than the specific surface runoff time series. The specific surface melt and runoff of most areas are better correlated with their immediate neighbours to the east or the west sides. The northern areas (W-N1, W-N2, E-N and E-LB; Fig. 7) and northern islands (SSI and Joi) show very similar specific surface melt and runoff temporal behaviours; the differences strongly reflect the elevation profiles. E-N shows a higher correlation with SSI (0.91) and Joi (0.91) than W-N1 (0.86 and 0.74, respectively). E-LC correlates better with E-LB, although the absolute amounts are considerably lower for E-LC as compared to E-LB. E-S correlates better with W-S than any other region, showing that there is a more pronounced climatic difference, in terms of interannual variability, between the regions in the E-LC latitudinal range.

The distribution of the surface melt and surface runoff along the elevation profiles reveals that more than 90% of the specific surface melt (specific surface runoff) is produced at elevations between 0 m and 500 m (400 m). This proportion decreases with elevation in all regions, except for the E-LC area. In this area, SM/A is higher in the elevation range of 100–200 m than in 0–100 m. The occurrence of foehn-type winds in this area leads to higher temperatures near the border with the grounding line, increasing melt.

Specific surface runoff is better distributed along the profile, and 90% occurs below an altitude of 400 m. The SSI and the Joi also show similar distribution patterns. The W-Wi and the W-S have 45% and 50% of specific surface melt, respectively, restricted to 0–100 m. The W-MB shows 90% of specific surface runoff restricted to 0–200 m. The greatest difference is found between the northern regions (E-N, E-LB, W-N1, W-N2, SSI and Joi) and the southwestern regions (W-S, W-MB and W-Wi). E-S has a distribution with characteristics between these extremes. E-LC is a special case, where more melt is produced between 100–200 m a.s.l. than between 0–100 m a.s.l., as a result of foehn-type winds.

Discussion

The high correlation between ERAID-derived and weather stations-derived PDDs demonstrates the consistency of the temporal variability of the modelled PDDs. On the other hand, very high RMSEs show that the PDDs' absolute values are not well represented by

https://doi.org/10.1017/S0954102018000391 Published online by Cambridge University Press

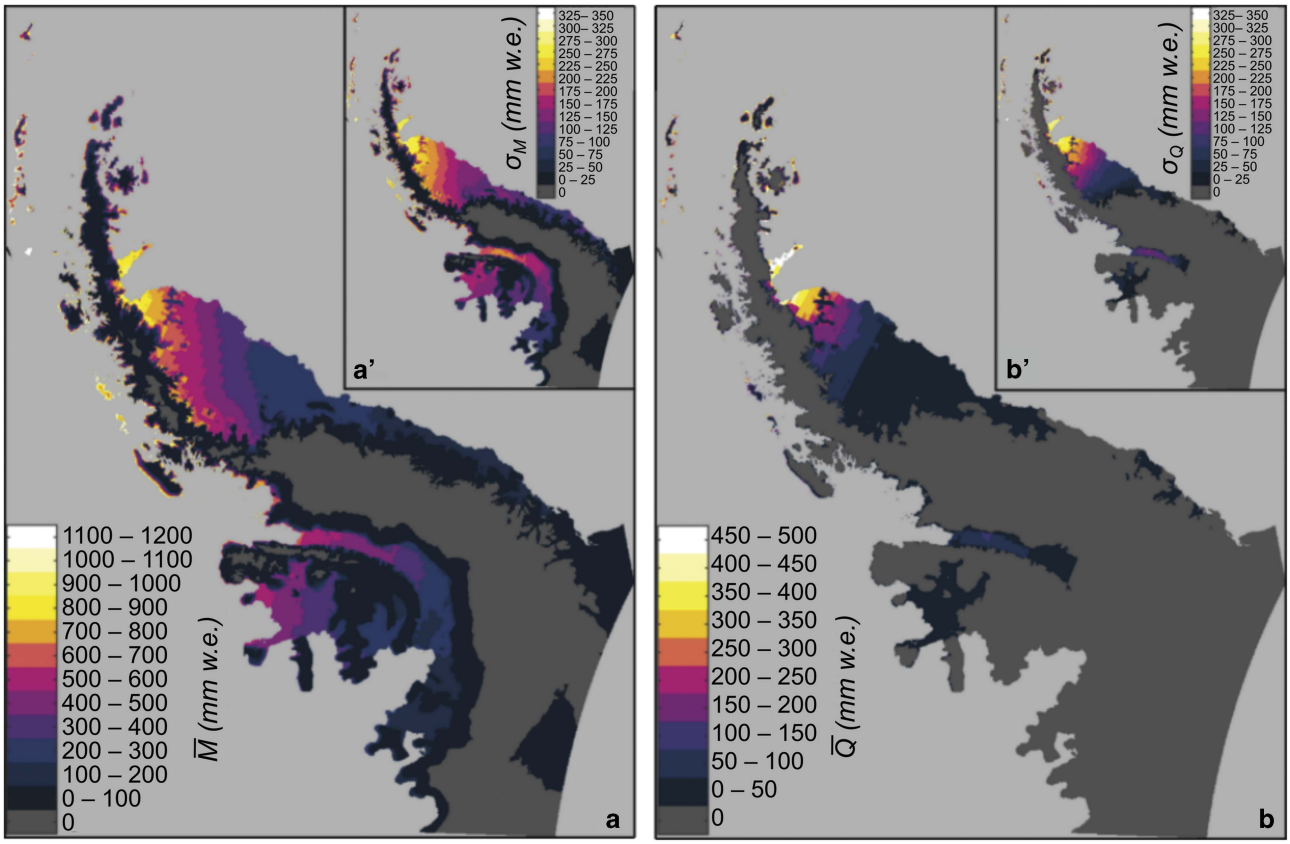

Fig. 6. Maps showing: **a**. mean surface melt ($\overline{M}$) and its standard deviation (σ_M, a') over the 1980–2014 period and **b**. the mean surface runoff ($\overline{Q}$) and its standard deviation (σ_Q, b') over the same period.

ERAID. An overestimation of air temperature over Antarctica has been recognized in previous ERA datasets (van de Berg *et al.* 2005), which is also observed in this study.

The comparative analysis between the ERAI-derived mean melt duration and the QuickSCAT-derived mean melt duration (Barrand *et al.*, 2013) showed that the first is underestimated on high-slope areas and overestimated on the northern tip of the Larsen C Ice Shelf. The terrain slope is a major difficulty for atmospheric models and even for remote sensing data processing. Therefore, a worse performance in high-slope areas is expected. Aside from the observation that the northern Larsen C mean melt duration overestimation occurs in flat areas, it may also be a topography-related problem. The north-western Larsen C is influenced by foehn-type winds, whose proper modelling is highly dependent on accurate representation of terrain elevation.

However, it is also worth noting that Luckman *et al.* (2014) compared Envisat/ASAR melt duration maps with the same QuickSCAT-derived data (Barrand *et al.*, 2013), and found melt durations up to 25 days longer than the latter. The authors attribute this difference to the different spatial resolution of both datasets in the region of Larsen C influenced by foehn-type winds. This suggests that perhaps the QuickSCAT reference data is actually underestimating the melt duration in Larsen C, which would indicate that the mean melt duration found in the present study is less overestimated.

The approach used here for tuning the melt factor to ERAID PDDs using *in situ* ablation measurements allowed for a compensation of the PDDs' overestimation. Both the surface melt temporal variability and absolute surface melt values are consistent with the SR50 measurements. The 80 mm w.e. underestimation over 40 days is acceptable, particularly considering that a simple approach applied to global reanalysis data was used. A small underestimation and good correspondence with SL2 ablation measurements were also found. The comparisons with integrated SMB from Hurd Peninsula and Glaciar Bahía del Diablo show that the results presented here are reliable for a regional-scale analysis on the northern AP. However, it should also be noted that there was no quantitative melt or surface mass balance data to assess the quality of the results for more southern sites on the AP.

A remaining bias from the PDD overestimation not compensated for by the melt factor tuning would result in a larger melt area. However, the spatial distribution of

https://doi.org/10.1017/S0954102018000391 Published online by Cambridge University Press

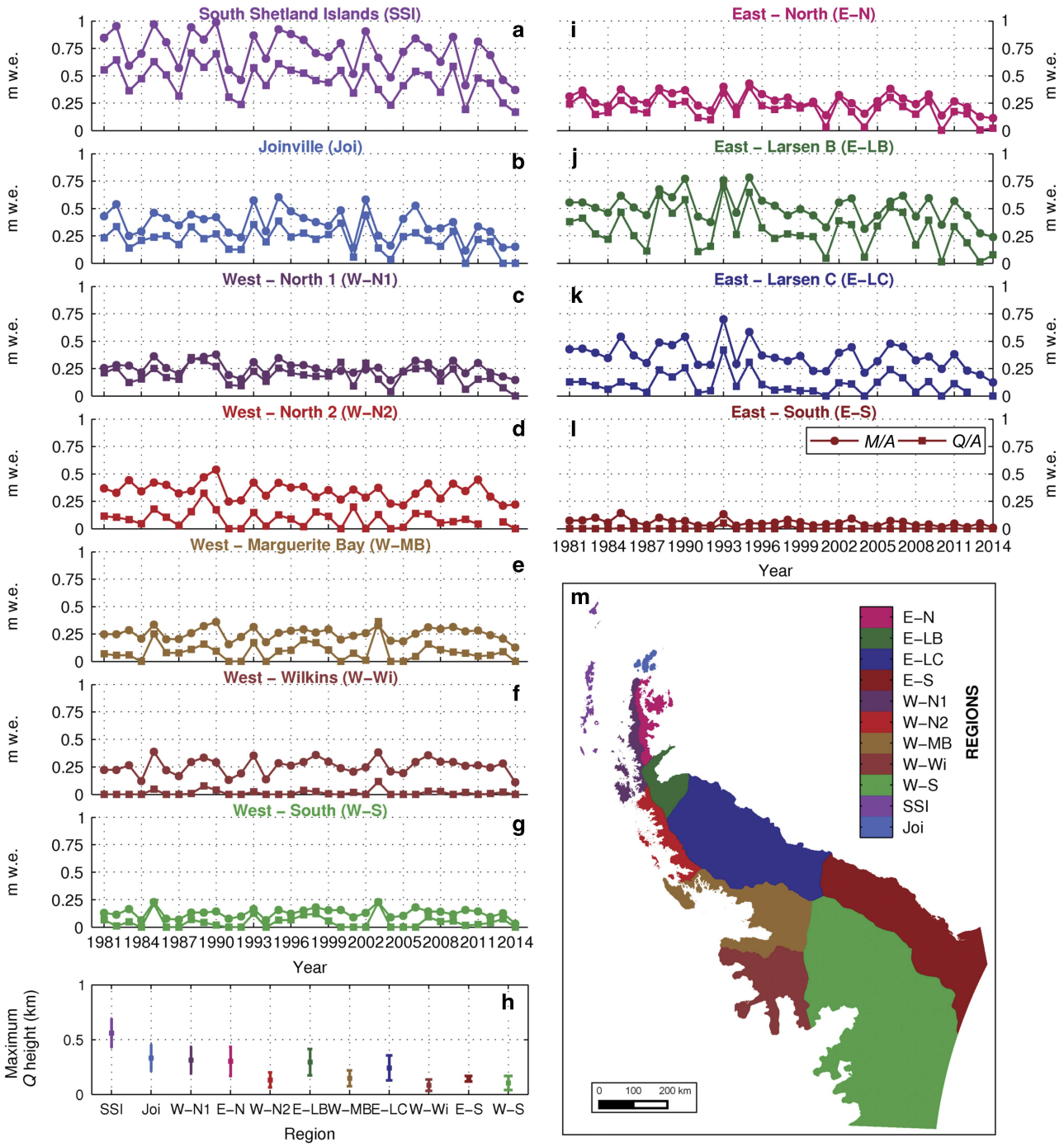

Fig. 7. Specific surface melt (M/A) and surface runoff (Q/A) over the Antarctic Peninsula: **a.** to **k.** show the M/A (continuous line, circles) and Q/A (continuous line, squares) time series separated for each AP region; **l.** shows the mean and standard deviation of the surface runoff maximum elevation in each region; map **m.** delimits each region.

PDDs is in agreement with recent work addressing the melt occurrence in AP through QuickSCAT and regional modelling (Kuipers Munneke *et al.* 2012, Barrand *et al.* 2013, Trusel *et al.* 2013, van Wessem *et al.* 2016). In some regions, the data in this study indicate a smaller melt area, which can be attributed to the enhanced resolution of the grid after the ERAI temperature downscaling. QuickSCAT data have spatial resolution of 5 km and RACMO2.3 of 5.5 km, whereas temperatures in this work were downscaled to a 200 m x 200 m grid.

Both surface melt and surface runoff spatial distribution and time series are generally in good agreement with the most recent studies addressing surface melt patterns in the AP (Tedesco & Monaghan

https://doi.org/10.1017/S0954102018000391 Published online by Cambridge University Press

2009, Kuipers Munneke *et al.* 2012, Barrand *et al.* 2013, Trusel *et al.* 2013, Välisuo *et al.* 2014, van Wessem *et al.* 2016), but the absolute values are higher than those presented by previous studies. Nevertheless, comparisons of surface melt derived from RACMO with 27 km resolution against QuickSCAT derived data showed an underestimation of SM, melt onset date and melt season duration by RACMO (Kuipers Munneke *et al.* 2012, Barrand *et al.* 2013, Trusel *et al.* 2013). Van Wessem *et al.* (2016) present estimates of surface melt provided by RACMO with 5.5 km resolution that are considerably smaller than those obtained by the previous model version. Comparisons of QuickSCAT-derived melt area on Larsen C against higher resolution Envisat-ASAR derived data further suggest that even QuickSCAT-derived melt area is underrepresented in the region. Such discrepancies between the different studies depict the high uncertainties involved in modelling mass balance terms in the Antarctic Peninsula.

The effects of foehn-type winds are visible in the distributed mean surface melt, contrasting with their poor representation in previous modelling studies (Kuipers Munneke *et al.* 2012, van Wessem *et al.* 2016). In general, the surface melt time series presented here agrees well with the temporal behaviour of the surface melt time series estimated by Kuipers Munneke *et al.* (2012) for the AP. In spite of the uncertainties associated with the approach used in the work discussed here, the results are consistent with direct field measurements (Figs 2 & 3).

Wouters *et al.* (2015) found a total mass loss of 300 Gt from 2000–2014. The study comprised the grounded portion of the AP southern sector. During the same period, and considering the grounded area of the entire AP, losses by surface runoff (SR) were 95 Gt. The contributions of the mass losses by SR to glacier thinning and possible sea level rise are thus small compared to ice flux acceleration and increased calving. Nevertheless, the role of the floating areas as a direct freshwater source to the adjacent ocean is remarkable. While they comprise only 24% of the total area, they produce 68% of the mean SR and 61% of the mean SM. Additionally, the fate of the liquid water is different from the fate of the ice when entering the ocean and it impacts the physico-chemical characteristics and the biota of the water differently.

The AP floating area has decreased by 18% since 1950 (Cook & Vaughan 2010). This reduction is progressively advancing southwards. The sea level rise around the AP, predominantly driven by steric expansion (Rye *et al.* 2014), suggests that the oceanic forcing will continue to lead to further and more dramatic ice shelf disintegration. In the future, it is likely that the melting area of the AP will be further reduced. Both Larsen C and the Wilkins Ice Shelf are the main surface melt and surface runoff sources and are partially unstable. Jansen *et al.* (2015) predicted that the Larsen C would undergo a large calving event caused by the development and propagation of a rift; this started on 12 January 2017 and reduced its area to approximately 90% of the pre-collapse size (Hogg & Gudmundsson 2017). After a large breakup event in February 2008, the 3100 km^2 of the northern portion of the Wilkins Ice Shelf was at risk of collapse (Braun *et al.* 2009). A narrow ice bridge collapsed later, in April 2009 (Humbert *et al.* 2010). Consequently, ice shelf breakups may reduce the absolute amounts of water input to the ocean in the form of surface runoff.

The accumulation rate on the AP has doubled since 1850 (Thomas *et al.* 2008), which, according to the Pfeffer *et al.* (1991) approach, increases meltwater retention. Nevertheless, Abram *et al.* (2013) showed that surface melt intensified much faster. By their analysis, the melt intensity recorded in the ice core increased from 0.5% to 4.9% over the 20th century. The grounded area presently retains an average of 91% of the SM, which will reduce if the observed trends continue; this may lead to an increase in the maximum height where surface runoff occurs and an increase in SR intensity at lower elevations.

It is possible to differentiate the specific surface melt and runoff time series in the 11 regions, even though the model is fed by global reanalysis data. The temperature downscaling using altitudinal lapse-rate variations in space and time allowed for an East–West differentiation in the northern tip of the AP. The W-N2 region lies on the same latitudinal range of E-LB, and it shows specific surface melt and runoff approximately 50% lower than the latter region. The difference may be explained by topographical control (E-LB has a mean elevation 330 m lower) and smaller altitudinal temperature lapse rates on the east side of the AP (Morris and Vaughan, 2003; this study).

The regional analysis of the altitudinal distribution of the specific surface melt and runoff revealed that they are determined, concomitantly, by the latitudinal range and East−West climatic differences. Though the western side is warmer, in the southwestern regions the specific surface melt and runoff are less uniformly distributed over the topographic profile due to the cold climate and higher temperature altitudinal lapse rates. Due to higher accumulation rates in the west, SR is even more restricted to low-elevation areas.

Two positive anomalies for both surface melt and surface runoff, widespread through all regions, took place in 1993 and 2006. They coincide with the highest melt index and melt extent found by Tedesco & Monaghan (2009) for the entire Antarctic continent and are associated with the Southern Annular Mode (SAM) and Southern Oscillation Index (SOI) negative anomalies. It demonstrates that the AP surface melt and surface runoff are closely linked to global climatic patterns and oscillations but remain poorly understood on the local spatial scales.

https://doi.org/10.1017/S0954102018000391 Published online by Cambridge University Press

Conclusions

Using the global reanalysis ERAI, the present researchers ran a PDD-based model for surface melt and surface runoff estimation, calibrated and validated with local measurements. The results are in good agreement with previous local, regional and continental studies and can be used to reasonably investigate the combined influence of latitudinal, longitudinal and elevation differences along the Antarctic Peninsula on the spatiotemporal variability of surface melt and surface runoff. The ERAI-derived distributed PDDs presented here are strongly correlated with weather station-derived PDDs. By applying a melt factor of 5.4 mm PDD^{-1}, good agreement with local measurements of SM was found.

The entire 1981–2014 period averages are 75 Gt (surface melt) and 9 Gt (surface runoff), with a very high interannual variability ($\sigma_M = 54$ Gt and $\sigma_Q = 8$ Gt). Although previous studies have found an exponential relation between PDDs and annual mean air temperature, the present work observed that the PDDs' interannual variability (and thereafter the amount of surface melt) is not well represented by the mean air temperature. Maximum values occurred in 1985 for surface melt (129 Gt) and 1993 for surface runoff (40 Gt). Since 2008, both variables have shown persistently negative anomalies, with minimum absolute values occurring in 2014 (surface melt = 26 Gt, surface runoff = 0.37 Gt). Nevertheless, no statistically significant temporal trends are present in the time series discussed here.

From 1996–2002, persistent negative anomalies are observed only for surface runoff. During this period, surface melt retention was always above 95% on the post-2002 floating ice areas. It is suggested that this persistent high retention may be linked to the Larsen B breakup mechanisms that took place in 2002. The post-2002 floating ice areas are responsible for a surface runoff average of 68% on the AP, highlighting their key importance to coastal hydrography as a freshwater source.

By dividing the AP into 11 regions, it can be observed that both the largest specific surface melt and runoff occur in the South Shetlands Islands, followed by the vicinity of the Larsen B Ice Shelf. This finding reveals the importance of the elevation and climatic differences between the western and eastern sides of the AP. Due to the Larsen C Ice Shelf, the east side has a flatter elevation profile, but generally also a smaller altitudinal decrease rate in temperature, and lower accumulation rates than the west side, resulting in higher specific surface melt and runoff in the east, despite the higher warming trends recorded in weather stations located in the west.

The large discrepancies among studies considering the same area and period indicate that further efforts are required to provide a better spatial distribution of field-measured surface mass balance data. The same recommendation can be made for weather stations. The discrepancies are possibly due to the high complexity of global, regional and local climatic forcing combined with the equally complex internal structure of the snow and ice layers.

Acknowledgements

Funding for this work was provided by EU FP7-PEOPLE-2012-IRSES IMCONet grant 318718, the Brazilian Coordination for the Improvement of Higher Education Personnel (CAPES) and the Brazilian National Institute of Science and Technology of the Cryosphere (INCT da Criosfera). M.B. was also funded via the German Research Foundation (grants BR2105/9-1 and BR2105/13-1). The RAMP DEM was kindly provided by NSIDC. Weather stations data were downloaded from NOAA at the website http://www.ncdc.noaa.gov/. ERA-Interim data were provided by the ECMWF. The surface mass balance data of Vega Island were kindly provided by Dr Sebastian Marinsek. The World Glacier Monitoring System distributes the surface mass balance data of Livingston Island, which are provided by Prof Dr Francisco Navarro. The authors would like to thank Prof Dr Francisco Navarro and the anonymous reviewer for their detailed revision and suggestions to improve the quality of this work.

Author contribution

J.C. conducted all data analyses and wrote major parts of the paper. M.B. and B.M. provided *in situ* reference data. N.E.B. provided the QuickSCAT-derived melt maps. J.C.S., A.B.S. and W.C.M. contributed to the data analysis and writing of the paper. J.C., J.A.-N. and M.B. jointly led the study. All authors contributed to and revised the manuscript. B.M. was funded by Russian Antarctic Expedition and IAEA project INT5153.

Details of data deposit

The new data presented in this paper will be archived at the PANGAEA data server (www.pangaea.de). PANGAEA is an information system hosted by the Alfred Wegener Institute, Helmholtz Center for Polar and Marine Research (AWI) and the Center for Marine Environmental Sciences, University of Bremen (MARUM).

References

Abram, N.J., Mulvaney, R., Wolff, E.W., Triest, J., Kipfstuhl, S., Trusel, L.D., Vimeux, F., Fleet, L. & Arrowsmith, C. 2013. Acceleration of snow melt in an Antarctic Peninsula ice core during the twentieth century. *Nature Geoscience*, **6**, 10.1038/ngeo1787.

Barrand, N.E., Vaughan, D.G., Steiner, N., Tedesco, M., Kuipers Munneke, P., Van Den Broeke, M.R. & Hosking, J.S. 2013. Trends in Antarctic Peninsula surface melting conditions from observations and regional climate modeling. *Journal of Geophysical Research: Earth Surface*, **118**, 10.1029/2012JF002559.

Braithwaite, R.J. & Zhang, Y. 2000. Sensitivity of mass balance of five Swiss glaciers to temperature changes assessed by tuning a degree-day model. *Journal of Glaciology*, **46**, 7–14.

Braun, M. & Hock, R. 2004. Spatially distributed surface energy balance and ablation modelling on the ice cap of King George Island (Antarctica). *Global and Planetary Change*, **42**, 10.1016/j.gloplacha.2003.11.010.

Braun, M., Humbert, A. & Moll, A. 2009. Changes of Wilkins Ice Shelf over the past 15 years and inferences on its stability. *The Cryosphere Discussions*, **2**, 10.5194/tcd-2-341-2009.

Braun, M., Saurer, H., Vogt, S., Simoes, J.C. & Gossmann, H. 2001. The influence of large-scale atmospheric circulation on the surface energy balance of the King George Island ice cap. *International Journal of Climatology*, **21**, 10.1002/joc.563/pdf.

Cape, M.R., Vernet, M., Skvarca, P., Marinsek, S., Scambos, T. & Domack, E. 2015. Foehn winds link climate-driven warming to ice shelf evolution in Antarctica. *Journal of Geophysical Research - Atmospheres*, **120**, 10.1002/2015JD023465.

Cook, A.J. & Vaughan, D.G. 2010. Overview of areal changes of the ice shelves on the Antarctic Peninsula over the past 50 years. *The Cryosphere*, **4**, 10.5194/tc-4-77-2010.

Dierssen, H.M., Smith, R.C. & Vernet, M. 2002. Glacial meltwater dynamics in coastal waters west of the Antarctic Peninsula. *Proceedings of the National Academy of Sciences of the United States of America*, **99**, 10.1073/pnas.032206999.

Fürst, J.J., Durand, G., Gillet-Chaulet, F., Tavard, L., Rankl, M., Braun, M. & Gagliardini, O. 2016. The safety band of Antarctic ice shelves. *Nature Climate Change*, **6**, 10.1038/nclimate2912.

Gesch, D.B., Verdin, K.L. & Greenlee, S.K. 1999. New land surface digital elevation model covers the Earth. *Eos, Transactions of American Geophysical Union*, **80**, 69–70.

Hock, R. 2003. Temperature index melt modelling in mountain areas. *Journal of Hydrology*, **282**, 10.1016/S0022-1694(03)00257-9.

Hock, R., De Woul, M., Radic, V. & Dyurgerov, M. 2009. Mountain glaciers and ice caps around Antarctica make a large sea-level rise contribution. *Geophysical Research Letters*, **36**, 10.1029/2008GL037020.

Hodson, A., Nowak, A., Sabacka, M., Jungblut, A., Navarro, F., Pearce, D., Ávila-Jimenez, M.L., Convey, P. & Vieira, G. 2017. Climatically sensitive transfer of iron to maritime Antarctic ecosystems by surface runoff. *Nature Communications*, **8**, 10.1038/ncomms14499.

Hogg, A.E. & Gudmundsson, G.H. 2017. Impacts of the Larsen-C Ice Shelf calving event. *Nature Climate Change*, **7**, 10.1038/nclimate3359.

Humbert, A., Gross, D., Müller, R., Braun, M., Van De Wal, R.S.W., Van Den Broeke, M.R., Vaughan, D.G. & Van De Berg, W.J. 2010. Deformation and failure of the ice bridge on the Wilkins Ice Shelf, Antarctica. *Annals of Glaciology*, **51**, 10.3189/172756410791392709.

Huybrechts, P. & Oerlemans, J. 1990. Response of the Antarctic ice sheet to future greenhouse warming. *Climate Dynamics*, **5**, 93–102.

Jansen, D., Luckman, A.J., Cook, A., Bevan, S., Kulessa, B., Hubbard, B. & Holland, P.R. 2015. Brief communication: newly developing rift in Larsen-C Ice Shelf presents significant risk to stability. *The Cryosphere*, **9**, 10.5194/tc-9-1223-2015.

Kienteca Lange, P., Tenenbaum, D.R., Tavano, V.M., Paranhos, R. & Campos, L. de S. 2014. Shifts in microphytoplankton species and cell size at Admiralty Bay, Antarctica. *Antarctic Science*, **27**, 10.1017/S0954102014000571.

Kuipers Munneke, P., Picard, G., Van Den Broeke, M.R., Lenaerts, J.T.M. & Van Meijgaard, E. 2012. Insignificant change in Antarctic snowmelt volume since 1979. *Geophysical Research Letters*, **39**, 10.1029/2011GL050207.

Liu, H., Jezek, K.C., Li, B. & Zhao, Z. 2015. RADARSAT Antarctic mapping project digital elevation model, version 2. Boulder, Colorado: National Snow and Ice Data Center, Distributed Active Archive Center. Digital media.

Liu, H., Wang, L. & Jezek, K.C. 2006. Spatiotemporal variations of snowmelt in Antarctica derived from satellite scanning multichannel microwave radiometer and special sensor microwave imager data (1978–2004). *Journal of Geophysical Research*, **111**, 10.1029/2005JF000318.

Luckman, A., Elvidge, A., Jansen, D., Kulessa, B., Kuipers Munneke, P., King, J. & Barrand, N. 2014. Surface melt and ponding on Larsen-C Ice Shelf and the impact of föhn winds. *Antarctic Science*, **26**, 625–635.

Marinsek, S. & Ermolin, E. 2015. 10-year mass balance by glaciological and geodetic methods of Glaciar Bahía del Diablo, Vega Island, Antarctic Peninsula. *Annals of Glaciology*, **56**, 141–146, 10.3189/2015AoG70A958.

Mavlyulov, B.R. 2014. Balans massy l'da lednikovogo kupola Bellingshausen v 2007–2012 (o. King-Dzordz, Udznye Shetlandskie ostrova, Antarctica) (Ice mass balance of Bellingshausen Dome in 2007–2012 (King George Island, South Shetland Islands, Antarctica)). *Led I Sneg* (*Ice and Snow*), **1**, 27–34.

Moline, M.A., Claustre, H., Frazer, T.K., Schofield, O. & Vernet, M. 2004. Alteration of the food web along the Antarctic Peninsula in response to a regional warming trend. *Global Change Biology*, **10**, 10.1111/j.1365-2486.2004.00825.x.

Morris, E.M. & Vaughan, D.G. 2003. Spatial and temporal variation of surface temperature on the Antarctic Peninsula and the limit of viability of ice shelves. *Antarctic Research Series*, **79**, 10.1029/AR079p0061.

Navarro, F.J., Jonsell, U.Y., Corcuera, M.I. & Martín-Español, A. 2013. Decelerated mass loss of Hurd and Johnsons Glaciers, Livingston Island, Antarctic Peninsula. *Journal of Glaciology*, **59**, 10.3189/2013JoG12J144.

Nędzarek, A. 2008. Sources, diversity and circulation of biogenic compounds in Admiralty Bay, King George Island, Antarctica. *Antarctic Science*, **20**, 10.1017/S0954102007000909.

Oliva, M., Navarro, F., Hrbáček, F., Hernández, A., Nývlt, D., Pereira, P., Ruiz-Fernández, J. & Trigo, R. 2017. Recent regional climate cooling on the Antarctic Peninsula and associated impacts on the Cryosphere. *Science of the Total Environment*, **580**, 10.1016/j.scitotenv.2016.12.030.

Osmanoglu, B., Navarro, F.J., Hock, R., Braun, M. & Corcuera, M. I. 2014. Surface velocity and mass balance of Livingston Island ice cap. *The Cryosphere*, **8**, 10.5194/tc-8-1807-2014.

Pfeffer, W.T., Meier, M.F. & Illangasekare, T.H. 1991. Retention of Greenland runoff by refreezing: implications for projected future sea level change. *Journal of Geophysical Research*, **96**, 10.1029/91JC02502.

Pritchard, H.D., Ligtenberg, S.R.M., Fricker, H.A., Vaughan, D. G., van den Broeke, M.R. & Padman, L. 2012. Antarctic ice-sheet loss driven by basal melting of ice shelves. *Nature*, **484**, 10.1038/nature10968.

Rau, F. & Braun, M. 2002. The regional distribution of the dry-snow zone on the Antarctic Peninsula north of 70°S. *Annals of Glaciology*, **34**, 10.3189/172756402781817914.

Rye, C.D., Naveira Garabato, A.C., Holland, P.R., Meredith, M. P., George Nurser, A.J., Hughes, C.W., Coward, A.C. & Webb, D. J. 2014. Rapid sea-level rise along the Antarctic margins in response to increased glacial discharge. *Nature Geoscience*, **7**, 10.1038/ngeo2230.

Scambos, T., Hulbe, C. & Fahnestock, M. 2003. Climate-induced ice shelf disintegration in the Antarctic Peninsula. *Antarctic Research Series*, **79**, 79–92.

Schloss, I.R., Abele, D., Moreau, S., Demers, S., Bers, A.V., González, O. & Ferreyra, G.A. 2012. Response of phytoplankton dynamics to 19-year (1991−2009) climate trends in Potter Cove (Antarctica). *Journal of Marine Systems*, **92**, 10.1016/j.jmarsys.2011.10.006.

Skvarca, P., De Angelis, H. & Ermolin, E. 2004. Mass balance of "Glaciar Bahía del Diablo", Vega Island, Antarctic Peninsula. *Annals of Glaciology*, **39**, 10.3189/172756404781814672.

Steig, E.J., Schneider, D.P., Rutherford, S.D., Mann, M.E., Comiso, J.C. & Shindell, D.T. 2009. Warming of the Antarctic ice-sheet surface since the 1957 international geophysical year. *Nature*, **457**, 10.1038/nature08286.

Tedesco, M. & Monaghan, A.J. 2009. An updated Antarctic melt record through 2009 and its linkages to high-latitude and tropical climate variability. *Geophysical Research Letters*, **36**, 10.1029/2009GL039186.

Thomas, E.R., Marshall, G.J. & McConnell, J.R. 2008. A doubling in snow accumulation in the western Antarctic Peninsula since 1850. *Geophysical Research Letters*, **35**, 10.1029/2007GL032529.

Torinesi, O., Fily, M. & Genthon, C. 2003. Variability and trends of the summer melt period of Antarctic ice margins since 1980 from microwave sensors. *Journal of Climate*, **16**, 10.1175/1520-0442(2003)016<1047:VATOTS>2.0.CO;2.

Trenberth, K.E., Jones, P.D., Ambenje, P., Bojariu, R., Easterling, D., Klein Tank, A., Parker, D., *et al*. 2007. Observations: surface and atmospheric climate change. *In* solomon, S., qin, D., manning, M., chen, Z., marquis, M., averyt, K.B., tignor, M. & miller, H.L., *eds. Climate change 2007: The physical science basis. Contribution of working group I to the fourth assessment report of the intergovernmental panel on climate change*. Cambridge: Cambridge University Press, 1009 pp.

Trusel, L.D., Frey, K.E., Das, S.B., Munneke, P.K. & Van Den Broeke, M.R. 2013. Satellite-based estimates of Antarctic surface meltwater fluxes. *Geophysical Research Letters*, **40**, 10.1002/2013GL058138.

Turner, J., Colwell, S.R., Marshall, G.J., Lachlan-Cope, T.A., Carleton, A.M., Jones, P.D., Lagun, V., Reid, P. A. & Iagovkina, S. 2005. Antarctic climate change during the last 50 years. *International Journal of Climatology*, **25**, 10.1002/joc.1130.

Turner, J., Lu, H., White, I., King, J.C., Phillips, T., Hosking, J.S., Bracegirdle, T.J., Marshall, G.J., Mulvaney, R. & Deb, P. 2016. Absence of 21st century warming on Antarctic Peninsula consistent with natural variability. *Nature*, **535**, 10.1038/nature18645.

Välisuo, I., Vihma, T. & King, J.C. 2014. Surface energy budget on Larsen and Wilkins ice shelves in the Antarctic Peninsula: results based on reanalyses in 1989-2010. *The Cryosphere*, **8**, 10.5194/tc-8-1519-2014.

Van de Berg, W.J., van den Broeke, M.R., Reijmer, C.H. & van Meijgaard, E. 2005. Characteristics of the Antarctic surface mass balance (1958−2002) using a regional atmospheric climate model. *Annals of Glaciology*, **41**, 97–104.

van Wessem, J.M., Ligtenberg, S.R.M., Reijmer, C.H., van de Berg, W.J., van den Broeke, M.R., Barrand, N.E., Thomas, E.R., Turner, J., Wuite, J., Scambos, T.A. & van Meijgaard, E. 2016. The modelled surface mass balance of the Antarctic Peninsula at 5.5 km horizontal resolution. *The Cryosphere*, **10**, 271–285.

Vaughan, D.G. 2006. Recent trends in melting conditions on the Antarctic Peninsula and their implications for ice-sheet mass balance and sea level. *Arctic, Antarctic and Alpine Research*, **38**, 147–152.

Vaughan, D.G., Marshall, G.J., Connolley, W.M., Parkinson, C., Mulvaney, R., Hodgson, D. A., King, J.C., Pudsey, C.J. & Turner, J. 2003. Recent rapid regional climate warming on the Antarctic Peninsula. *Climatic Change*, **60**, 10.1023/A:1026021217991.

Wouters, B., Helm, V., Flament, T., Wessem, J.M. Van, Ligtenberg, S.R.M. & Bamber, J.L. 2015. Dynamic thinning of glaciers on the Southern Antarctic Peninsula. *Science*, **348**, 899–904.

Zwally, H.J., Abdalati, W., Herring, T., Larson, K., Saba, J. & Steffen, K. 2002. Surface melt−induced acceleration of Greenland Ice-Sheet flow. *Science*, **297**, 218–223.